

## PROBABILISTIC SEISMIC DEMAND ANALYSIS AT A NEAR-FAULT SITE USING GROUND MOTION SIMULATIONS BASED ON A STOCHASTIC-KINEMATIC EARTHQUAKE SOURCE MODEL

N. Luco<sup>1</sup>, P. M. Mai<sup>2</sup>, C. A. Cornell<sup>3</sup>, and G. C. Beroza<sup>4</sup>

### ABSTRACT

With the objective of assessing the seismic performance of a structure at a specified site, Probabilistic Seismic Demand Analysis (PSDA) combines a ground motion hazard curve with the results of nonlinear dynamic analyses to compute a structural demand hazard curve. Customarily, the ground motion hazard curve used in PSDA is in terms of spectral acceleration, but to ensure the accuracy of PSDA for a structure at a near-fault site, it may be necessary to employ an alternative ground motion intensity measure (*IM*). The ground motion hazard curve in terms of an alternative *IM*, however, may not be available or readily computed via Probabilistic Seismic Hazard Analysis (PSHA). In this paper, a ground-motion-simulation-based approach is demonstrated that can be used to compute the hazard at a site in terms of any *IM*. In fact, the simulation-based approach is used to compute an "exact" structural demand hazard curve that is compared with the results of the far less computationally intensive PSDA. For a steel moment-resisting building at a near-fault site, the accuracy of PSDA is demonstrated to be dependent upon the *IM* employed.

### Motivation

Probabilistic Seismic Demand Analysis (PSDA) is an approach for computing the mean annual frequency of exceeding a specified seismic demand for a given structure at a designated site (Cornell, 1996). The Pacific Earthquake Engineering Research (PEER) center has recently adopted PSDA as a "foundation on which (structural) performance assessment can be based" (<http://peer.berkeley.edu/news/2000spring/index.html>). In fact, PSDA is already at the core of two recent performance-based seismic guidelines, namely FEMA 350-353 (2001) for steel moment-resisting frame (SMRF) buildings and the ISO Offshore Structures Standard (Younan *et al.*, 2001). As expressed mathematically in Eq. 1, PSDA convolves  $G_{DMIM}$ , the probability of exceeding the specified structural demand given (i.e., conditioned on knowing) the ground motion intensity, with  $\lambda_{IM}$ , the ground motion hazard at the designated site. The conditional probability  $G_{DMIM}$  is customarily estimated using demand measure (*DM*) results from nonlinear dynamic analyses (NDA's) of the given structure under a suite of earthquake ground motions.

---

<sup>1</sup> Ph.D. Candidate, Dept. of Civil and Environmental Engineering, Stanford University, Stanford, CA 94305-4020  
(currently: Analysis Engineer, Applied Insurance Research, 425 Market St., Suite 2200, San Francisco, CA 94105)

<sup>2</sup> Ph.D. Candidate, Dept. of Geophysics, Stanford University, Stanford, CA 94305

<sup>3</sup> Professor, Dept. of Civil and Environmental Engineering, Stanford University, Stanford, CA 94305-4020

<sup>4</sup> Professor, Dept. of Geophysics, Stanford University, Stanford, CA 94305

$$\lambda_{DM} = \int G_{DM|IM} |d\lambda_{IM}| \quad (1)$$

Conventionally, the ground motion intensity measure (*IM*) is taken to be the spectral acceleration at the fundamental period of the structure of interest (with a damping ratio of 5%). In this case, the ground motion hazard  $\lambda_{IM}$  is either readily available (e.g., from the U.S. Geological Survey) or commonly computed. Recent studies, however, have demonstrated that other *IM*'s may be more suitable when carrying out PSDA for tall, long period buildings and/or at near-fault sites (Luco & Cornell, 2001). For example, Luco & Cornell (2001) introduce an alternative *IM* that incorporates an inelastic spectral displacement and thereby may ensure the accuracy of Eq. 1 for  $\lambda_{DM}$  at near-fault sites. Unlike for spectral acceleration, though, the ground motion hazard at a site in terms of this alternative *IM* is not currently available or readily computable. New attenuation relations for inelastic spectral displacement that are applicable near a fault need to be developed in order to compute  $\lambda_{IM}$  via Probabilistic Seismic Hazard Analysis (PSHA). While such attenuation relations are potentially an area of future research, in the meantime an alternate approach to PSHA that does not employ an attenuation relation is demonstrated in this paper. The alternate approach can be used to compute the ground motion hazard at site in terms of any *IM*. In fact, the approach can be applied to compute  $\lambda_{DM}$  "directly," rather than via PSDA. As demonstrated in this paper, however, PSDA requires many fewer NDA's and is equally accurate if a suitable *IM* is employed.

## Introduction

In this paper, PSDA is carried out for the 9-story SMRF building designed for Los Angeles conditions as part of the SAC Steel Project (Phase II). The first and second mode periods of a two-dimensional model of the building are  $T_1=2.23\text{sec}$  and  $T_2=0.82\text{sec}$ . Refer to (Luco, 2002) for more details. The building (hereafter referred to as LA9) is hypothetically located at a University of California at Berkeley (UCB) site located near the Hayward-Rogers Creek (HRC) Fault system. The structural demand measure (i.e., *DM*) of interest is the maximum (over the height of the building) peak (over time) inter-story drift angle (i.e., story drift divided by story height), denoted as  $\theta_{\max}$ . Via the alternate (to PSHA) approach summarized in the following section, the ground motion hazard used in PSDA (i.e.,  $\lambda_{IM}$ ) is computed in terms of two different ground motion intensity measures. The first, denoted  $IM_{1E}$ , is proportional to first-mode spectral acceleration, whereas the second, denoted  $IM_{1\&2E}$ , takes into account second-mode frequency content and the effects of inelasticity on structural response (Luco & Cornell, 2001). The alternate approach is also used to directly compute a drift demand hazard curve (i.e.,  $\lambda_{DM}$ ) that is compared with the results of PSDA using each of the two different *IM*'s considered.

## Procedure

The approach demonstrated in this paper for computing the ground motion hazard at a near-fault site makes use of (i) mean annual rates of recurrence for "characteristic events" on local faults, as estimated by the U.S.G.S. Working Group on California Earthquake Probabilities (1999), and (ii) earthquake records for such events simulated at the site by Beroza & Mai (2001) with a stochastic finite-source rupture model. The simulated earthquake records for each characteristic event reflect the randomness associated with several aspects of fault rupture, so the

conditional (given the characteristic event) probability distribution of any  $IM$  can simply be estimated from the values of  $IM$  for the simulated earthquake records. With the conditional distribution of  $IM$  and the mean annual recurrence rate for each of the characteristic events considered, the ground motion hazard at the site can be computed. Note that non-characteristic events (i.e., events of smaller magnitude) are not considered here, but their contribution to the ground motion hazard at a site could also be computed via a similar approach. At high levels of ground motion, though, the contribution of non-characteristic events to the ground motion hazard may be comparatively small.

### Characteristic Events on the HRC Fault system

A schematic representation of the HRC Fault system (and the nearby UCB site) is depicted in Fig. 1. Although there are several other earthquake fault systems in the San Francisco Bay Region that pose a threat (e.g., San Andreas), the HRC Fault system is the closest to the UCB site (3.6 km) and is the only one likely to induce rupture directivity effects there. As a result, only the HRC Fault system is considered in this paper.

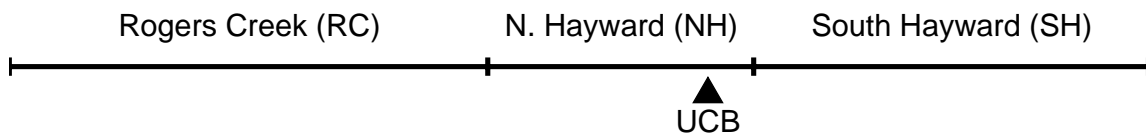


Figure 1. Schematic representation of HRC Fault system and UCB site (map view).

The three segments of the HRC Fault system shown in Fig. 1 (i.e., RC, NH, and SH) are delimited by the 1999 U.S.G.S. Working Group on California Earthquake Probabilities (hereafter abbreviated as WG99). The characteristic events considered in this paper, referred to as "rupture sources" by WG99, are earthquakes that rupture one or more of these three fault segments. For the six possible contiguous HRC rupture source, the WG99 estimates of the mean annual rates of recurrence  $s$  are listed in Table 1.

Table 1. Mean annual recurrence rates, rupture areas, and mean moment magnitudes for potential rupture sources on the HRC Fault system (from WG99).

Rupture Source	Mean Rate [1/yr]	Area [km <sup>2</sup> ]	Mean $M_w$
RC	$3.49 \times 10^{-3}$	63 x 12	7.06
SH	$2.69 \times 10^{-3}$	52 x 12	6.88
NH	$2.58 \times 10^{-3}$	35 x 12	6.63
SH+NH	$1.91 \times 10^{-3}$	87 x 12	7.08
NH+RC	$0.51 \times 10^{-3}$	98 x 12	7.21
SH+NH+RC	$0.22 \times 10^{-3}$	150 x 12	7.37

## Simulated Earthquake Records at UCB Site

For each of the six rupture sources listed above in Table 1, a stochastic fault-rupture model that is suitable for generating near-field (and far-field) ground motions is used to simulate 30 earthquake records at the UCB site (Beroza & Mai, 2001). The input for the kinematic rupture model includes (i) the spatial distribution of slip on the fault plane, (ii) the slip velocity time function (uniform over the fault plane), which is assumed to be a simple boxcar function of length  $\tau_r$ , known as the rise time, and (iii) the rupture propagation velocity  $v_r$  expressed as a percentage of the local shear wave velocity. The location of the hypocenter on the fault plane is also input. As detailed in the subsections below, the spatial distribution of slip and the rise time depend (stochastically) on the seismic moment prescribed for each rupture simulation, or equivalently on the moment magnitude,  $M_w$ . In turn,  $M_w$  is a random function of the area of the rupture source. Independently of  $M_w$ , the location of the hypocenter on the rupture plane is also randomized. The rupture velocity, however, is deterministically specified as 85% of the local shear wave velocity.

It is important to note that, for the example in this paper, the simulated earthquake records have been scaled up by a factor of two. Without scaling, the inelastic spectral displacement that is a part of the alternative intensity measure  $IM_{1I\&2E}$  is in fact elastic for many of the simulated earthquake records (i.e., the elastic limit is not surpassed). Even for the remainder of simulated earthquake records, the "equal displacements rule" tends to apply if the earthquake records are not scaled, such that the inelastic spectral displacement in  $IM_{1I\&2E}$  is about the same as its elastic counterpart. Scaling the earthquake records by a factor of two, on the other hand, makes it possible to demonstrate the effects of employing (in PSDA) a ground motion intensity measure that incorporates an inelastic spectral displacement. Note that the scaling of the earthquake records can perhaps be interpreted as considering a structure that has been designed according to a governing drift limit twice as large as that used to design the LA9 building.

### Earthquake Moment Magnitude given Rupture Source Area

Following the assumptions of WG99, the earthquake moment magnitude (i.e.,  $M_w$ ) for each rupture simulation is drawn from a normal (i.e., Gaussian) probability distribution of  $M_w$  given  $A$ , the area of the rupture source. The mean  $M_w$  (and given  $A$ ) for each of the six HRC rupture sources is listed above in Table 1, and the standard deviation of  $M_w$  given  $A$  is assumed to equal 0.12 (both according to WG99).

### Spatial Distribution of Slip on Rupture Plane given Seismic Moment

As detailed in (Mai & Beroza, 2001), the spatial distribution of slip on the rupture plane for each simulation is generated as a random field with correlation lengths that depend on the seismic moment, or equivalently on  $M_w$ . Of course, the mean slip (i.e., spatially averaged) is also directly related to seismic moment. It is important to randomize the spatial distribution of slip because it can have a profound effect on the nature of nearby ground motions. For example, large slip "asperities" between the hypocenter and a nearby site can result in pulse-like ground motions (e.g., Aagaard *et al.*, 2001).

## Rise Time given Seismic Moment

Assumed to be uniform over the rupture plane, the slip rise time  $\tau_r$  is drawn from a lognormal distribution given the seismic moment (or, equivalently, given  $M_w$ ). The median  $\tau_r$  is taken to be the average of two equations derived by Somerville *et al.* (1999) for  $\tau_r$  as a function of  $M_w$ . Based on the data used by Somerville *et al.* to develop these equations, the dispersion of  $\tau_r$  given  $M_w$  is estimated as 0.40. According to Somerville (2000), the rise time is strongly correlated with the predominant period of a pulse-like ground motion.

## Location of Hypocenter

Like the spatial distribution of slip and the rise time, the location of the hypocenter on a rupture plane can significantly affect the ground motions at a nearby site, due to the effects of rupture directivity. For this reason, the location of the hypocenter is randomized according to independent probability distributions for its depth and its along-strike position. As detailed in (Luco, 2002), the assumed distribution of depth places the hypocenter in the lower half of the rupture area. Independently, the assumed distribution of along-strike position assigns more probability to unilateral (rather than bilateral) rupture; however, the far ends of the fault plane are left as a buffer in which the hypocenter cannot be located.

## Ground Motion Hazard at UCB Site

As explained above, the simulated earthquake records for each rupture source (i.e., characteristic event of given area) reflect the randomness associated with various aspects of fault rupture. Consequently, these simulated earthquake records can be used to estimate, for each rupture source, the conditional probability of exceeding a particular level of ground motion at a site. Weighting these exceedance probabilities by the mean annual recurrence rate for each rupture source and summing over all rupture sources generates an estimate of the ground motion hazard, as expressed mathematically in Eq. 2.

$$\lambda_{IM} = \sum_{RS} G_{IM|RS} \nu_{RS} \quad (2)$$

The ground motion hazard  $\lambda_{IM}$ , recall, is strictly the mean annual frequency of exceeding a specified value of  $IM$ . The term  $\nu_{RS}$  denotes the mean annual rate (or frequency) of recurrence for the rupture source  $RS$ ; recall that  $\nu_{RS}$  has been estimated by WG99 for the six HRC rupture sources considered in this paper (as listed in Table 1). Lastly, the term  $G_{IM|RS}$  denotes the conditional probability of exceeding a specified value of  $IM$ , given an earthquake from  $RS$ . Here,  $G_{IM|RS}$  is estimated from the values of  $IM$  for the 30 earthquake records simulated for each  $RS$  (assuming a lognormal distribution of  $IM$  given  $RS$ ).

Using Eq. 2, the ground motion hazard at the UCB site in terms of  $IM_{1E}$  and of  $IM_{1I\&2E}$  is computed; the results are illustrated in Fig. 2. Recall that the simulated earthquake records considered here have been scaled up by a factor of two. Since both ground motion intensity measures are estimates of  $\theta_{max}$  (in units of radians), their hazard curves are plotted concurrently. Note that at relatively small values of the  $IM$ 's (i.e., 0.01 to 0.02 radians), the

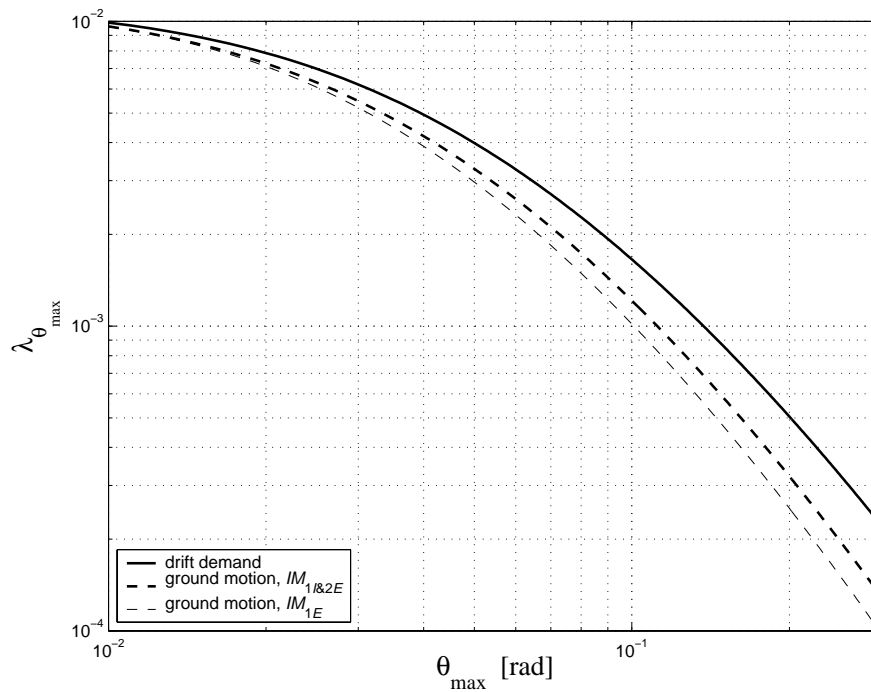


Figure 2. Ground motion hazard (in terms of  $IM_{1E}$  or  $IM_{1I\&2E}$ ) and "exact" drift demand (i.e.,  $\theta_{\max}$ ) hazard curves for the LA9 building model at the UCB site. Recall that the simulated earthquake records used to compute these hazard curves have been scaled up by a factor of two.

ground motion hazard in terms of  $IM_{1E}$  and  $IM_{1I\&2E}$  are nearly identical. This is because  $IM_{1E}$  and  $IM_{1I\&2E}$  are approximately equal in this range, for the following reasons: (i) at spectral displacements less than the yield displacement specified for  $IM_{1I\&2E}$ , the inelastic spectral displacement in  $IM_{1I\&2E}$  is actually elastic (like in  $IM_{1E}$ ), and (ii) the second mode contribution to  $IM_{1I\&2E}$  (and to  $\theta_{\max}$ ) happens to be insignificant for most of the simulated earthquake records because the maximum frequency considered is only 1.6hz. At relatively large values of the  $IM$ 's (i.e., greater than about 0.02 radians), on the other hand, the fact that the ground motion hazard in terms of  $IM_{1I\&2E}$  is larger than the hazard in terms of  $IM_{1E}$  indicates that the inelastic spectral displacements for the simulated earthquake records are, on average, larger than their elastic counterparts.

### Drift Demand Hazard for LA9 Building Model at UCB Site

The simulation-based approach demonstrated above for computing  $\lambda_{IM}$  can also be used to compute directly (i.e., without PSDA) a structural demand hazard curve (i.e.,  $\lambda_{DM}$ ), as demonstrated here for the LA9 building model at the UCB site. Applying the simulation-based approach to compute  $\lambda_{DM}$ , however, calls for NDA of the full multi-degree-of-freedom (MDOF) model of the building for all of the simulated earthquake records. In contrast, PSDA only requires NDA (of the MDOF building model) under a relatively small number of earthquake

records. This is because NDA is used in PSDA only to find the relationship between  $DM$  and  $IM$ , which has comparatively small dispersion. Of course, PSDA also makes use of an  $IM$  hazard curve for the designated site. As demonstrated below, the accuracy of PSDA in estimating  $\lambda_{DM}$  may depend on the intensity measure employed (e.g.,  $IM_{1I\&2E}$  versus  $IM_{1E}$ ).

### Simulation-Based Approach

The same approach used to compute the ground motion hazard curves in Fig.2 is also followed to compute a drift demand (here  $\theta_{\max}$ ) hazard curve, illustrated in Fig. 2 as well, for the LA9 building model at the UCB site. In doing so,  $\theta_{\max}$  is computed via NDA of the LA9 building model for all 180 of the simulated earthquake records (scaled up by a factor of two). This approach to computing a structural demand hazard curve is somewhat similar in concept to that developed by Collins *et al.* (1995). The resulting drift demand hazard curve is considered to be "exact," and will be compared with the results of PSDA in the following subsection. Note from Fig. 2 that the hazard curve for  $\theta_{\max}$  is larger than that for  $IM_{1I\&2E}$  or  $IM_{1E}$ , even in the elastic range (i.e., around 0.01 radians). The difference is due to both the bias of each  $IM$  in estimating  $\theta_{\max}$  and the dispersion of  $\theta_{\max}$  given  $IM$ . As demonstrated next, PSDA accounts for this bias and dispersion.

### PSDA Approach

As pointed out above, in computing the "exact" drift demand hazard via the simulation-based approach,  $DM$  (in this case  $\theta_{\max}$ ) from NDA of the LA9 building model has been computed for all 180 of the simulated earthquake records. Given the ground motion hazard at the UCB site (i.e.,  $\lambda_{IM}$  from Fig. 2), computing  $\lambda_{DM}$  via PSDA (i.e., Eq. 1) entails estimating the conditional complementary cumulative probability  $G_{DM|IM}$  with only a subset of these  $DM$  results (and the corresponding values of  $IM$ ). More specifically,  $G_{DM|IM}$  is customarily calculated by assuming that  $DM$  given  $IM$  is lognormally distributed. The requisite median (i.e., the exponential of the mean of the natural logs) and dispersion (i.e., the standard deviation of the natural logs) of  $DM$  given  $IM$  are estimated via a (log-log linear) regression of  $DM$  on  $IM$ . Because the dispersion of  $DM$  given  $IM$  is comparatively small (e.g., in relation to the dispersion of  $DM$  given  $RS$ ), a relatively small number of data points (i.e., earthquake records) are necessary to estimate the median  $DM$  given  $IM$  with adequate precision. As an example, the regressions of  $\theta_{\max}$  on  $IM_{1E}$  and on  $IM_{1I\&2E}$  using only the 30 earthquake records simulated for the SH+NH+RC rupture source are illustrated in Fig. 3 for the LA9 building model. The dispersion of  $\theta_{\max}$  given  $IM$  is denoted simply as  $\sigma$ , and the median  $\theta_{\max}$  given  $IM$  is equal to  $a \cdot IM$ . Note that  $\sigma$  is significantly smaller when  $IM_{1I\&2E}$  is employed rather than  $IM_{1E}$  (i.e.,  $\sigma = 0.17$  vs. 0.44), implying that the regression estimate of  $a$  is more precise when  $IM_{1I\&2E}$  is employed.

Using each of the six different sets of 30 simulated earthquake records, the resulting drift demand hazard curves computed via PSDA are illustrated in Fig. 4. Also shown in the figure is the "exact" drift demand hazard curve computed via the simulation-based approach. When  $IM_{1E}$  is employed in PSDA, note that the drift demand hazard curves differ significantly depending on which set of (simulated) earthquake records are used to estimate  $G_{DM|IM}$ . For example, the hazard

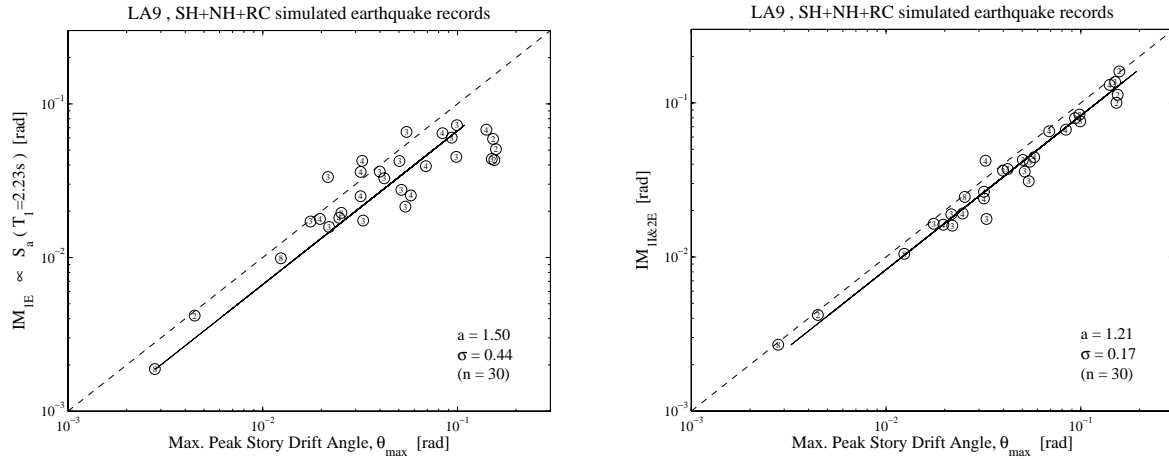


Figure 3. Regressions of  $\theta_{\max}$  (from NDA of the LA9 building model) on (a)  $IM_{1E}$  and (b)  $IM_{1I\&2E}$  for the earthquake records simulated for the SH+NH+RC rupture source (scaled up by a factor of two).

curves computed using the earthquake records simulated for the RC versus the SH+NH+RC rupture sources underestimate and overestimate, respectively, the "exact" drift demand hazard curve. At large drift demands (e.g.,  $\theta_{\max}=0.08\text{rad}$ ) the RC and SH+NH+RC estimates of the hazard (i.e., the mean rates) differ by almost a factor of two; conversely, the  $\theta_{\max}$  demands at low levels of hazard (e.g., about  $2 \times 10^{-3}$ ) differ by about a factor of 1.5. When  $IM_{1I\&2E}$  is employed, in contrast, the drift demand hazard curves computed via PSDA are approximately the same regardless of which set of earthquake records are used to estimate  $G_{DM|IM}$ . Moreover, the hazard curves computed using the "near-field" earthquake records simulated for the SH, NH, SH+NH, NH+RC, and SH+NH+RC rupture sources are very close to the "exact" drift demand hazard curve. The hazard curve computed using the "far-field" earthquake records simulated for the RC rupture source, however, mildly underestimates the "exact" solution (by about 20% in hazard and only 10% in drift). Using the near-field rather than the far-field earthquake records results in a more accurate estimate of the drift demand hazard because the hazard is dominated by the nearby rupture sources (i.e., other than RC).

### Conclusions

As demonstrated above, the accuracy of PSDA in computing a structural demand hazard curve ( $\lambda_{DM}$ ) can depend on the ground motion intensity measure ( $IM$ ) employed. For some intensity measures, like  $IM_{1E}$ , the PSDA estimate of  $\lambda_{DM}$  may depend on the choice of earthquake records used — in particular, using near-field versus far-field earthquake records can result in different estimates of  $\lambda_{DM}$ . Such an  $IM$  is termed "insufficient" by Luco & Cornell (2001). In contrast, a sufficient ground motion intensity measure, like  $IM_{1I\&2E}$ , tends to result in approximately the same estimate of  $\lambda_{DM}$  regardless of the set of earthquake records chosen. In the PSDA example carried out in this paper, even the drift demand hazard curves obtained using near-field versus far-field earthquake records differ by less than 20% when  $IM_{1I\&2E}$  is employed. A major disadvantage of employing  $IM_{1I\&2E}$  in PSDA, however, is that unlike for  $IM_{1E}$  (which is

(From Proceedings of the 7th U.S. National Conference on Earthquake Engineering held on July 21-25, 2002)

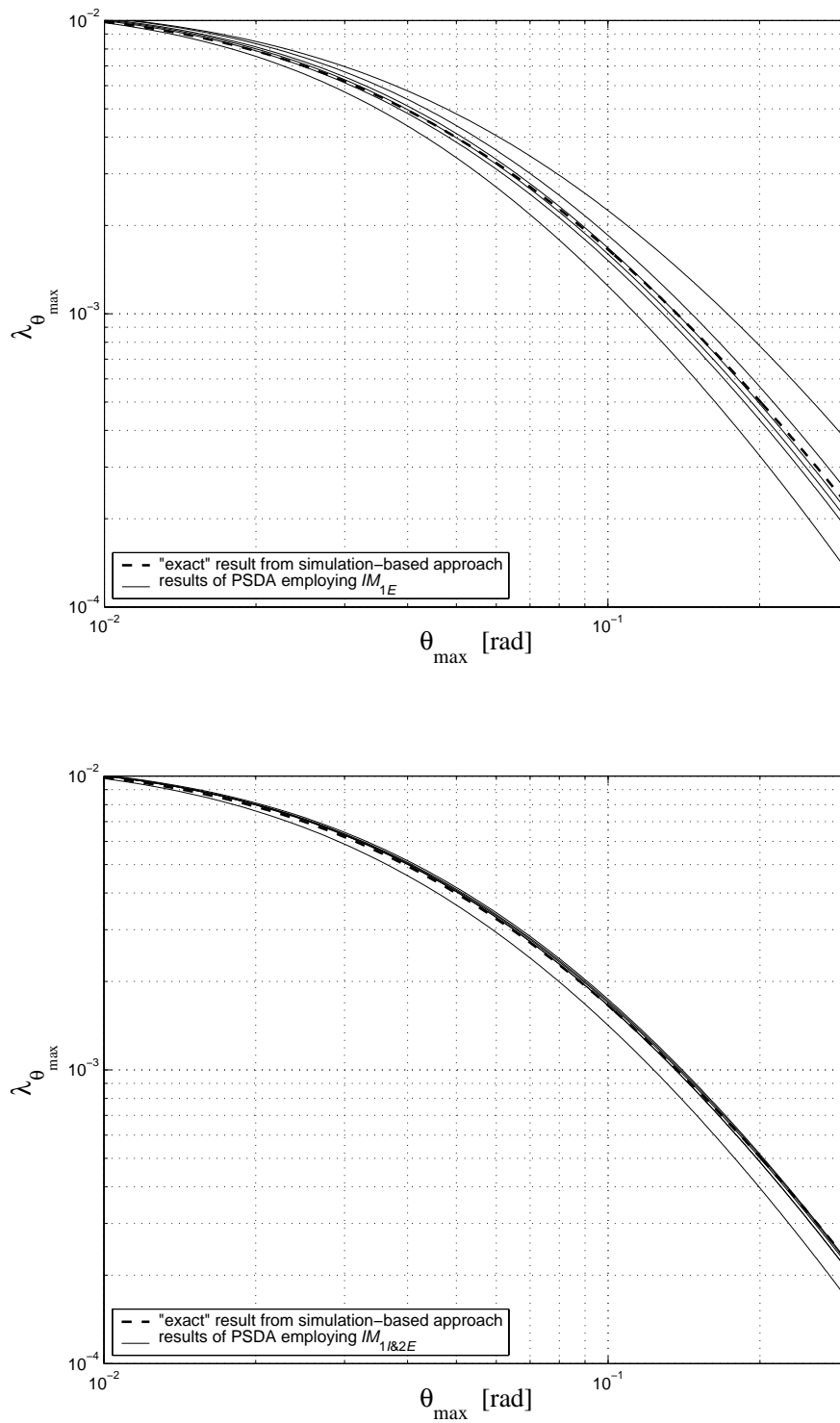


Figure 4. Drift demand hazard curves for the LA9 building model at the UCB site computed via PSDA using each of six different sets of simulated earthquake records and employing (a)  $IM_{1E}$  or (b)  $IM_{1\&2E}$  as the ground motion intensity measure. Recall that the simulated earthquake records used have been scaled up by a factor of two.

approximately proportional to spectral acceleration), an attenuation relation for  $IM_{1I&2E}$  does not exist. Consequently, PSHA cannot be performed to compute a ground motion hazard curve in terms of  $IM_{1I&2E}$ . The simulation-based approach demonstrated in this paper, though, can be applied to compute a ground motion hazard curve in terms of any  $IM$ , and hence to carry out PSDA using any ground motion intensity measure. Furthermore, the simulation-based procedure can be used to directly compute an "exact"  $\lambda_{DM}$  to compare with the results of PSDA. For the example presented in this paper, PSDA is demonstrated to be very accurate for a 9-story SMRF building at a near-fault site when a sufficient  $IM$  is employed and the earthquake records used reflect the dominant hazard.

### Acknowledgements

The authors gratefully acknowledge the financial support of the U.S.-Japan Cooperative Research in Urban Earthquake Disaster Mitigation Project (NSF 98-36) under grant number CMS-9821096.

### References

- Aagaard, B.T., J.F. Hall, and T.H. Heaton (2001). Characterization of near-source ground motions with earthquake simulations, *Earthquake Spectra* 17 (2), 177-207.
- Beroza, G.C., and P.M. Mai (2001). Personal communication.
- Collins, K.R., Y.K. Wen, and D.A. Foutch (1995). Investigation of alternative seismic design procedures for standard buildings, *Structural Research Series No. 600*, Univ. of Illinois, Urbana-Champaign.
- Cornell, C.A. (1996). Calculating building seismic performance reliability: a basis for multi-level design norms, *Proceedings of the Eleventh World Conference on Earthquake Engineering*, Mexico.
- Luco, N. (2002). Probabilistic seismic demand analysis, SMRF connection fractures, and near-source effects, *Ph.D. Thesis*, Dept. of Civil and Environmental Eng., Stanford University, California.
- Luco, N., and C.A. Cornell (2001). Structure-specific scalar intensity measures for near-source and ordinary earthquake ground motions, submitted to *Earthquake Spectra*.
- Mai, P.M., and G.C. Beroza (2001). A spatial random-field model to characterize complexity in earthquake slip, submitted to *Journal of Geophysical Research*.
- Somerville, P. *et al.* (1999). Characterizing crustal earthquake slip models for the prediction of strong ground motion, *Seismological Research Letters* 70 (1), 59-80.
- Somerville, P.G. (2000). Issue A – should near fault directivity be modeled in national ground motion mapping? *Second ATC-35 National Earthquake Ground Motion Mapping Workshop*.
- Working Group on California Earthquake Probabilities (1999). Earthquake probabilities in the San Francisco bay region: 2000 to 2030, *USGS Open-File Report 99-517*, Menlo Park, California.
- Younan, A., H. Banon, P. Marshall, C.B. Crouse, and C.A. Cornell (2001). An overview of the ISO seismic guidelines, *Proceedings of the Offshore Technology Conference*, Houston, Texas.